The Astrophysical Journal Letters, 746:L15 (7pp), 2012 February 20 doi:10.1088/2041-8205/746/2/L15

INTERACTIONS BETWEEN CORONAL MASS EJECTIONS VIEWED IN COORDINATED IMAGING AND IN SITU OBSERVATIONS

Ying D. Liu[1,2], Janet G. Luhmann[1], Christian Möstl[1,3,4], Juan C. Martinez-Oliveros[1], Stuart D. Bale[1], Robert P. Lin[1,5], Richard A. Harrison[6], Manuela Temmer[3], David F. Webb[7], and Dusan Odstrcil[8]
[1] Space Sciences Laboratory, University of California, Berkeley, CA 94720, USA; liuxying@ssl.berkeley.edu
[2] State Key Laboratory of Space Weather, National Space Science Center, Chinese Academy of Sciences, Beijing, China
[3] Institute of Physics, University of Graz, Austria
[4] Space Research Institute, Austrian Academy of Sciences, Graz, Austria
[5] School of Space Research, Kyung Hee University, Yongin, Gyeonggi 446-701, Republic of Korea
[6] Space Science and Technology Department, Rutherford Appleton Laboratory, Didcot, UK
[7] Institute for Scientific Research, Boston College, Newton, MA 02459, USA
[8] NASA Goddard Space Flight Center, Greenbelt, MD 20771, USA
Received 2011 November 15; accepted 2012 January 13; published 2012 January 30

ABSTRACT

The successive coronal mass ejections (CMEs) from 2010 July 30 to August 1 present us the first opportunity to study CME–CME interactions with unprecedented heliospheric imaging and in situ observations from multiple vantage points. We describe two cases of CME interactions: merging of two CMEs launched close in time and overtaking of a preceding CME by a shock wave. The first two CMEs on August 1 interact close to the Sun and form a merged front, which then overtakes the July 30 CME near 1 AU, as revealed by wide-angle imaging observations. Connections between imaging observations and in situ signatures at 1 AU suggest that the merged front is a shock wave, followed by two ejecta observed at *Wind* which seem to have already merged. In situ measurements show that the CME from July 30 is being overtaken by the shock at 1 AU and is significantly compressed, accelerated, and heated. The interaction between the preceding ejecta and shock also results in variations in the shock strength and structure on a global scale, as shown by widely separated in situ measurements from *Wind* and *STEREO B*. These results indicate important implications of CME–CME interactions for shock propagation, particle acceleration, and space weather forecasting.

Key words: shock waves – solar–terrestrial relations – solar wind – Sun: coronal mass ejections (CMEs)

Online-only material: animations, color figures

1. INTRODUCTION

Coronal mass ejections (CMEs) are large-scale expulsions of plasma and magnetic field from the solar atmosphere. One of the most intriguing questions concerning CMEs is how they interact with each other during their propagation in interplanetary space. CME–CME interactions are expected to be a frequent phenomenon near solar maximum when multiple CMEs can occur within one day, while their transit time from the Sun to the Earth is typically 4 days.

Interactions between CMEs are of importance for both space weather studies and basic plasma physics. First, CME–CME interactions can produce or enhance southward magnetic fields (e.g., Farrugia & Berdichevsky 2004; Wang et al. 2003), a key factor in geomagnetic storm generation (Dungey 1961; Gosling et al. 1991). Second, the interaction may reveal interesting shock physics in case a shock is overtaking a CME, including modifications in the shock strength, particle acceleration, and transport. In situ measurements usually show a depressed plasma β within interplanetary CMEs (ICMEs). The penetrating shock is likely to decay because of the enhanced Alfvén speed in the preceding ejecta. Efficiency in particle acceleration is expected to change due to modifications in the shock strength and structure by the preceding ejecta, and particles accelerated at the shock may be trapped by the closed magnetic fields within the preceding ejecta or guided along the helical field lines. (Gopalswamy et al. 2002 find a close association between CME interactions and solar energetic particle events, whereas Richardson et al. 2003 argue that the association is not statistically meaningful.) Third, the interaction implies significant energy and momentum transfer between the interacting CMEs where magnetic reconnection may take place. Under magnetic reconnection the two interacting flux systems may finally merge, leading to a phenomenon called "CME cannibalism" by Gopalswamy et al. (2001). This physical process would be very complex since CMEs are three-dimensional large-scale structures.

Studies of CME interactions so far are based on either coronagraph observations close to the Sun (Gopalswamy et al. 2001) or in situ measurements near the Earth (e.g., Burlaga et al. 2002; Wang et al. 2003; Farrugia & Berdichevsky 2004). Connections between imaging observations and in situ measurements have been lacking. As a result, details of the interacting process cannot be continuously followed and memory of the source conditions is lost. With the launch of the *Solar Terrestrial Relations Observatory* (*STEREO*; Kaiser et al. 2008), coordinated wide-angle imaging and in situ observations of CME interactions are feasible and can be performed from multiple vantage points. *STEREO* is comprised of two spacecraft with one preceding the Earth (*STEREO A*) and the other trailing behind (*STEREO B*). Each of the *STEREO* spacecraft carries an identical imaging suite, the Sun Earth Connection Coronal and Heliospheric Investigation (SECCHI; Howard et al. 2008), which can image a CME from its birth in the corona all the way to the Earth and beyond. *STEREO* also has several sets of in situ instrumentation, which provide in situ measurements of the magnetic field, energetic particles, and the bulk solar wind plasma (Luhmann et al. 2008; Galvin et al. 2008). At L1, *Wind* and *ACE* monitor

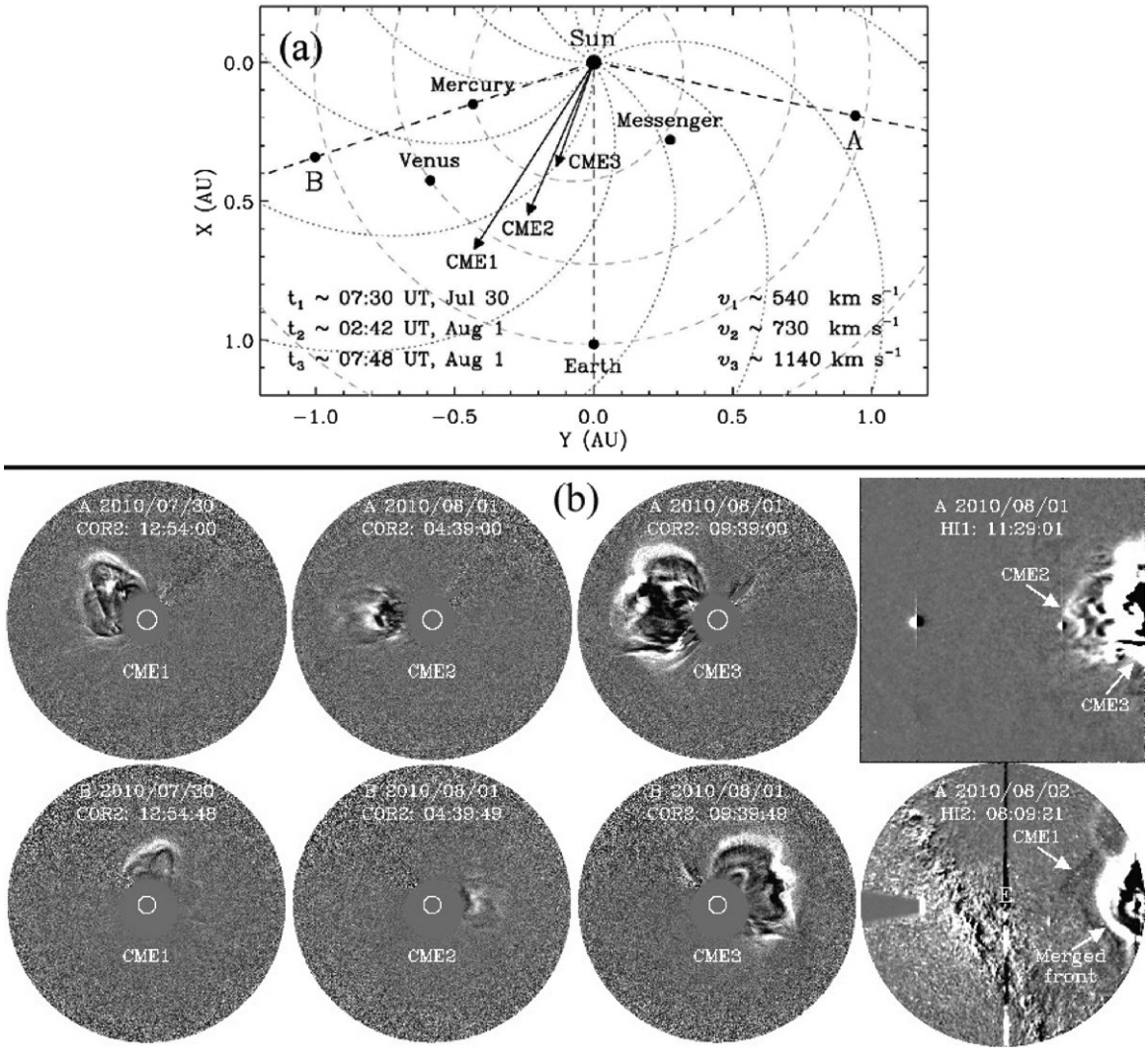

Figure 1. (a) Positions of the spacecraft and planets in the ecliptic plane on 2010 August 1. The gray dashed curves indicate the planetary orbits, and the dotted lines show Parker spiral magnetic fields. The arrows mark the propagation directions of the CMEs of interest obtained from a triangulation technique. The estimated CME speeds and launch times on the Sun are also given. (b) CME evolution observed by *STEREO*. The left three columns display COR2 images of the three CMEs viewed from *STEREO A* (upper) and *B* (lower) near simultaneously. The right column shows images from HI1 and HI2 of *STEREO A*, which indicate the scenario of CME–CME interactions. The position of the Earth is labeled E.

(Animations of this figure are available in the online journal.)

the near-Earth solar wind conditions, thus adding a third vantage point for in situ measurements.

Around 2010 August 1 the Sun exhibited substantial activities including filament eruptions, flares, and multiple CMEs (Schrijver & Title 2011; Harrison et al. 2012; Martinez-Oliveros et al. 2012; Temmer et al. 2012; C. Möstl et al. 2012, in preparation; D. F. Webb et al. 2012, in preparation), which provides a great opportunity to study CME–CME interactions. The focus of this Letter is to present the first study of CME interactions combining wide-angle imaging observations from *STEREO* with in situ measurements at 1 AU. The results obtained here are crucial for understanding CME–CME interactions as well as the complete picture of CME propagation from the Sun to the Earth.

2. OBSERVATIONS AND RESULTS

Figure 1(a) shows the configuration of the planets and spacecraft in the ecliptic plane on August 1. *STEREO A* and *B* are separated by about 149.°9 in longitude with a distance of 0.96 AU and 1.06 AU from the Sun, respectively. Also shown are the propagation directions of three CMEs of interest in the ecliptic plane determined from a geometric triangulation technique (see details below). The first CME (CME1) is launched from the Sun at about 07:30 UT on July 30 with a speed around 540 km s^{-1}, while the other two (CME2 and CME3) are launched at about 02:42 UT and 07:48 UT on August 1 with speeds around 730 km s^{-1} and 1140 km s^{-1}, respectively. The launch times are estimated by extrapolating the coronagraph observations of SECCHI back to the solar surface, and the speeds are obtained from linear fits to CME propagation distances before CME collisions (see below). A direct impression is that these CMEs may interact since their propagation directions are close to each other. CME2 and CME3 are expected to interact at distances not far from the Sun, while interactions of CME1 with the other two should take place much further from the Sun because its launch time is about 2 days earlier.

Figure 1(b) displays two synoptic views of the CMEs from *STEREO A* and *B*. Only data from the outer coronagraph (COR2) and the heliospheric imagers (HI1 and HI2) of SECCHI are shown. COR2 has a field of view (FOV) of 0.°7–4° around the

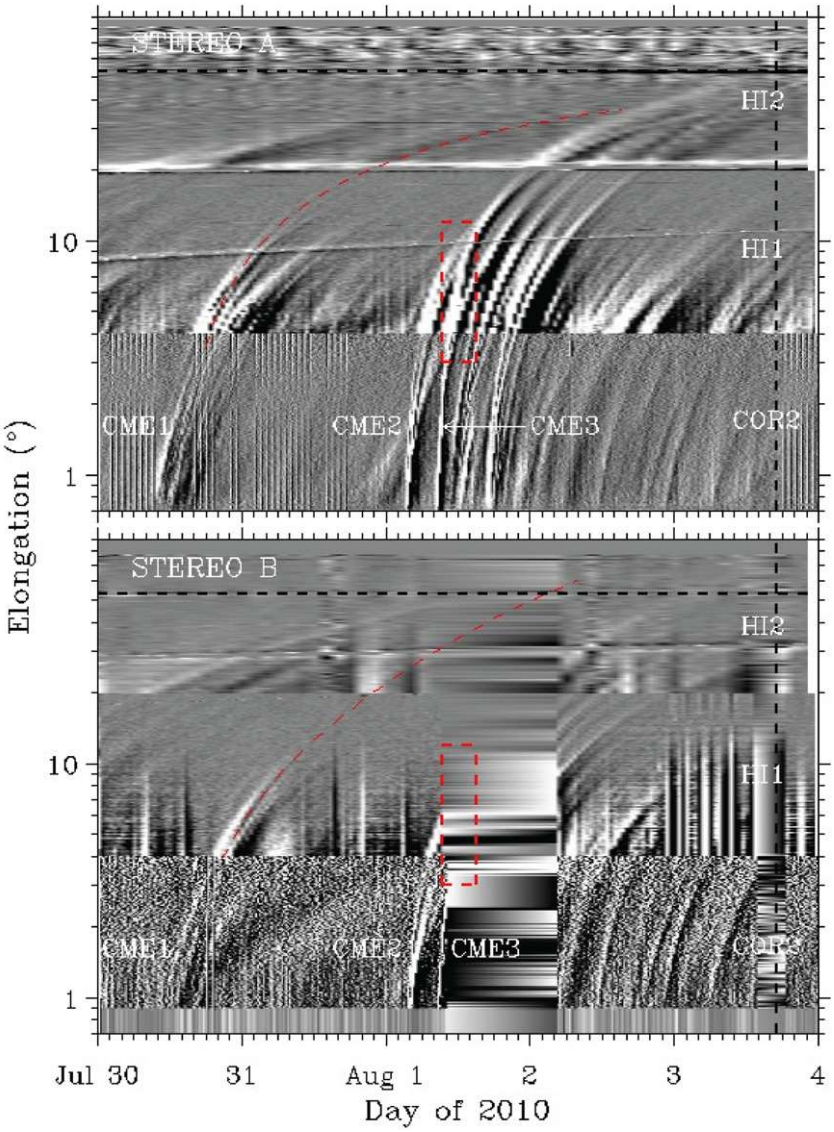

Figure 2. Time-elongation maps constructed from running difference images of COR2, HI1 and HI2 along the ecliptic plane for *STEREO A* (upper) and *B* (lower). Tracks associated with the three CMEs are indicated. The rectangular box marks the times and elongation angles of the interaction between CME2 and CME3. The vertical dashed line indicates the observed arrival time of a shock at the Earth, and the horizontal dashed line denotes the elongation angle of the Earth. The red curve shows the fit to the leading tracks of CME1 in HI1 and HI2.

(A color version of this figure is available in the online journal.)

Sun. HI1 has a 20° square FOV centered at 14° elongation from the center of the Sun while HI2 has a 70° FOV centered at 53.°7. HI1 and HI2 can observe CMEs to the vicinity of the Earth and beyond by using sufficient baffling to eliminate stray light (Harrison et al. 2008; Eyles et al. 2009). Note a data gap for *STEREO B* from 10 UT of August 1 to 04 UT of August 2. CME1 is largely north of the ecliptic plane but rotates and expands toward the plane. Spacecraft in the ecliptic plane will likely encounter its flank. CME2 and CME3 are propagating more along the ecliptic plane. CME3 is fast and energetic (1140 km s^{-1}), and it seems to overtake CME2 in the FOV of HI1. A merged front is formed from the interaction between CME2 and CME3. Connections with in situ signatures at 1 AU suggest that this merged front is a shock wave. CME1 is then overtaken by the merged front at elongations close to the Earth, as shown in HI2 of *STEREO A*.

Figure 2 shows the time-elongation maps, which are produced by stacking the running difference intensities of COR2, HI1, and HI2 within a slit around the ecliptic plane (e.g., Sheeley et al. 2008; Davies et al. 2009; Liu et al. 2010a). At least four CMEs occurred on August 1, whereas between July 30 and August 1 the Sun was relatively quiet. (There appears a weak feature ahead of CME2 in COR2 of *STEREO A*, which is produced by small plasma flows along a coronal streamer.) Harrison et al. (2012) provide an overview of the CMEs on August 1. As can be seen from the maps, tracks from CME2 and CME3 intersect, indicative of an interaction between these two events. Some of the tracks merge into a single one in the FOV of HI1, and later a bifurcation is observed. Presumably, the leading bifurcated feature is the shock wave, and the trailing one is another structure visible to *STEREO A* after the CME–CME interaction (also see Harrison et al. 2012 for more discussions on the bifurcated structures). There is a gap in *STEREO B* observations during the time of this interaction, but the tracks from both spacecraft before and after the data gap can be used to calculate the propagation direction and distance of

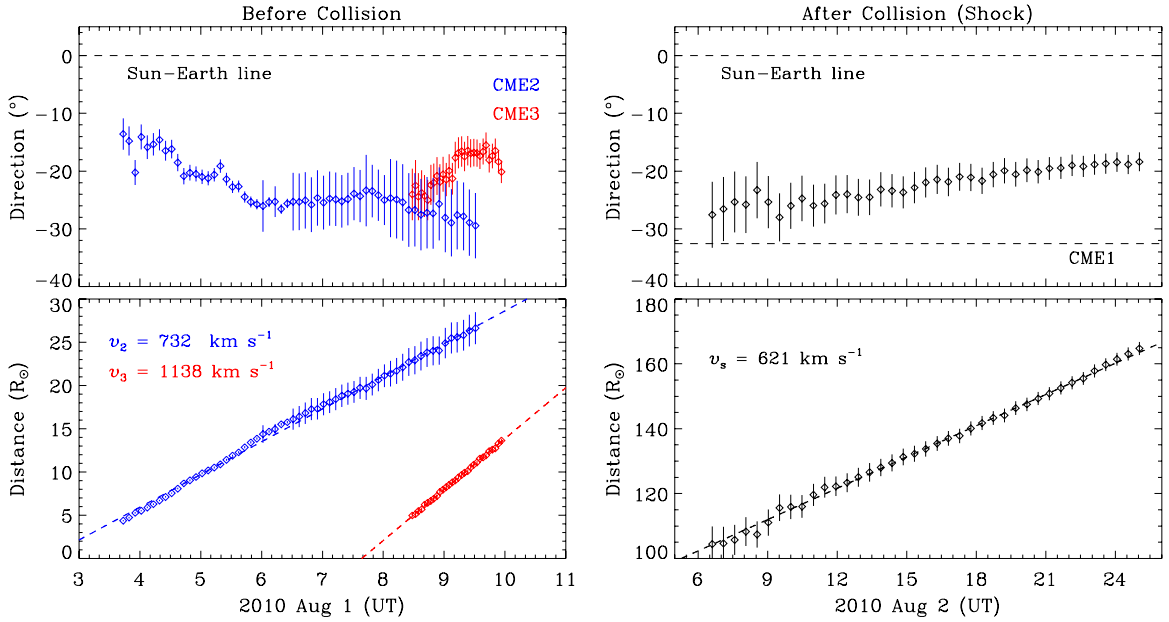

Figure 3. Propagation direction and radial distance derived from geometric triangulation before (left) and after (right) collision between CME2 and CME3. The lower dashed line in the top right panel indicates the propagation angle of CME1. Also shown are linear fits to the distances, together with the speeds obtained from the fits. (A color version of this figure is available in the online journal.)

corresponding features with a geometric triangulation method. Also shown in Figure 2 are fits to the leading tracks of CME1 in HI1 and HI2 by assuming a kinematic model with a constant speed and propagation direction (e.g., Sheeley et al. 2008). The fit is a rough representation of the tracks given its assumptions. The propagation direction determined from the track fitting is about 28° and 39° east of the Sun–Earth line for *STEREO A* and *B*, respectively. The extrapolated fit curves suggest that the interaction between CME1 and the merged front of CME2 and CME3 would probably occur around 1 AU.

The elongation angles along the tracks can be converted to radial distance and propagation direction using a geometric triangulation method developed by Liu et al. (2010a, 2010b). The technique has had success in tracking CMEs and connecting imaging observations with in situ signatures for various CMEs and spacecraft longitudinal separations (Liu et al. 2010a, 2010b, 2011; Möstl et al. 2010). We apply the technique to the leading features of the three CMEs as well as the merged front of CME2 and CME3. The resulting CME kinematics in the ecliptic plane are displayed in Figure 3. The propagation direction is converted to an angle with respect to the Sun–Earth line. If the angle is positive (negative), the CME feature would be propagating west (east) of the Sun–Earth line. The propagation angles show a variation with time, with an average value of −23° for CME2 and −19° for CME3 before their collision. The speed obtained from the linear fit to the distances is about 732 km s^{-1} and 1138 km s^{-1} for CME2 and CME3, respectively. These propagation angles and speeds are consistent with estimates from radio type II bursts (Martinez-Oliveros et al. 2012) and other various methods (Temmer et al. 2012). The merging between CME2 and CME3 is likely complete around 17 UT on August 1 at a distance of about 55 solar radii from the Sun, estimated by extrapolating the fits to the point where they intersect.

The kinematics of the merged front of CME2 and CME3 are shown in the right panels of Figure 3. The average propagation angle is about −22°, which has not changed much compared with those before the collision. The merged front can be tracked out to about 165 solar radii or 0.75 AU (without projection). The speed obtained from the linear fit to the distances is about 621 km s^{-1}, smaller than the speeds of both CMEs before their interaction. Note that this is the speed well after the interaction. While the main deceleration of the overtaking CME (CME3) is due to the interaction, the solar wind drag may also contribute to the slowdown (Temmer et al. 2012). The predicted arrival time of the merged front at the Earth, estimated from the linear fit, is about 17:36 UT on August 3. Also indicated in Figure 3 is the average propagation angle of CME1. Application of the triangulation technique to this CME gives propagation angles that show a transition from −12° to −40° with an average value of about −30° (not included in this Letter). This average propagation angle is consistent with the estimates from track fitting (−28° and −39° for *STEREO A* and *B*, respectively). The merged front of CME2 and CME3 would probably interact with CME1 given their similar propagation angles and large-scale structures.

Figure 4 shows the in situ measurements at *Wind*. Three ICMEs can be identified from the *Wind* data between August 3 and 5. A strong forward shock passed *Wind* at 17:04 UT on August 3. The predicted arrival time (17:36 UT) of the merged front of CME2 and CME3 is coincident with the shock passage at *Wind*, which suggests that the merged front in white-light images is the shock. The shock is overtaking a preceding ICME (ICME1) at 1 AU. The trailing boundary of ICME1 is mainly determined from the low proton β, while the leading boundary can be identified from the smooth, slightly enhanced magnetic field and depressed proton temperature (compared with the expected temperature) in addition to the proton β. Although shock compression can enhance the plasma density, temperature, and magnetic field, the plasma β may not change much. This is why we use the proton β to determine the trailing boundary of ICME1. ICME1 is also observed at *STEREO B* (see Figure 5), for which the rotation of the magnetic field components and proton β are used together to

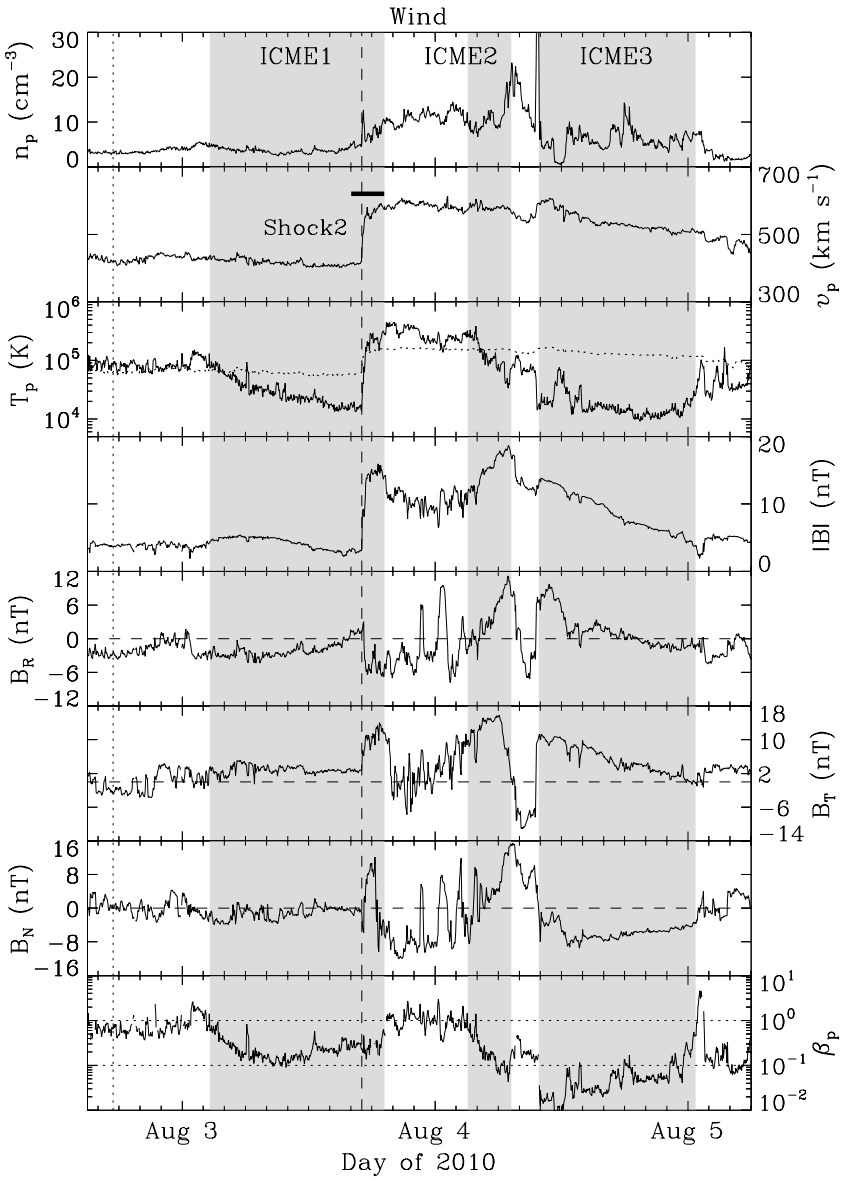

Figure 4. Solar wind plasma and magnetic field parameters observed at *Wind*. From top to bottom, the panels show the proton density, bulk speed, proton temperature, magnetic field strength and components, and proton β, respectively. The dotted curve in the third panel denotes the expected proton temperature from the observed speed. The shaded regions show the ICME intervals, and the vertical dashed line indicates the associated shock. The horizontal line in the second panel marks the predicted arrival time (with uncertainties) and speed of the merged front of CME2 and CME3 at the spacecraft. The predicted arrival time of CME1 is indicated by the vertical dotted line.

determine the boundaries. The predicted arrival time of CME1 is about 17:26 UT and 21:56 UT on August 2 at *Wind* and *STEREO B*, respectively, which has a close timing with the in situ measurements of ICME1. This suggests that ICME1 is the corresponding structure of CME1 at 1 AU. The fact that the shock is overtaking ICME1 is consistent with the imaging observations that indicate an interaction between CME1 and the merged front of CME2 and CME3 close to 1 AU. The predicted speed (about 621 km s^{-1}) of the shock is consistent with but slightly larger than observed at *Wind*. The shock is presumably slowed down by the interaction.

The shock significantly accelerates, compresses, and heats the preceding ejecta, as can be seen from Figure 4. First, the trailing edge of ICME1 is traveling faster than the leading edge (with a speed difference of about 170 km s^{-1} at *Wind*), as the trailing edge is downstream of the shock while the leading edge is upstream. As a result, the radial width of ICME1 is decreasing. After the shock has gone through the whole ejecta, the speed of every part of the ejecta would be increased, so ICME1 is essentially accelerated by the shock. The plasma density and magnetic field within the ejecta would also be enhanced because of the shock compression. Second, the proton temperature within ICME1 is low (only about 20,000 K upstream of the shock at *Wind*), which results in a large sound Mach number of the shock ($M_s \sim 15$). The observed temperature increases significantly across the shock (by a factor of about 15), which is expected as the heating by a hydrodynamic shock is proportional to M_s^2 although the magnetic field may reduce the heating somehow. MHD simulations of a shock overtaking a preceding ejecta seem to give similar results (e.g., Vandas et al. 1997; Schmidt & Cargill 2004; Lugaz et al. 2005; Xiong et al. 2006).

A similar scenario is observed at *STEREO B* (see Figure 5), but the measurements at this additional point indicate

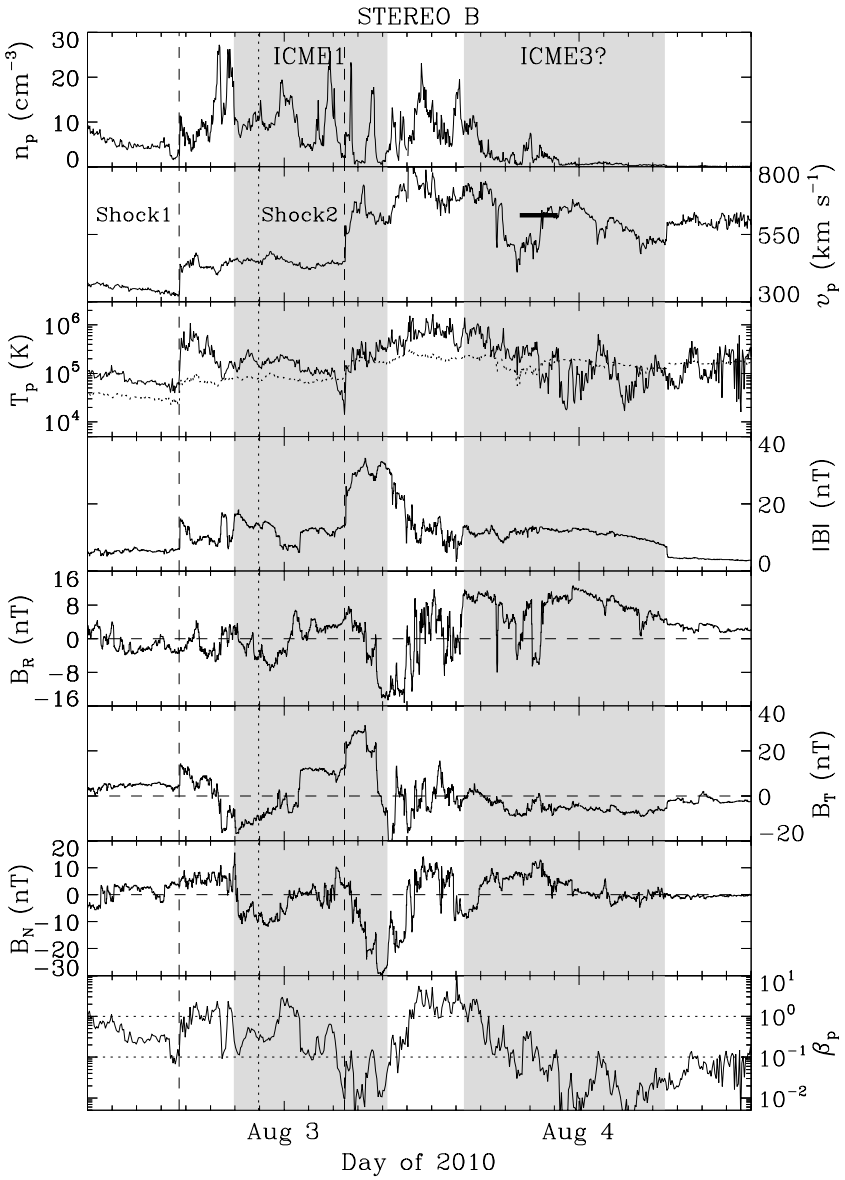

Figure 5. Similar to Figure 4, but for the measurements at *STEREO B*. ICME1 has a forward shock at *STEREO B*, while only a discontinuity is observed at *Wind*.

a significant distortion in both the shock strength and structure. First, the Alfvén speed upstream of the shock at *STEREO B* is about 150 km s^{-1}, much larger than that upstream the shock at *Wind* (about 40 km s^{-1}). This reduces the shock Alfvén Mach number, $M_A \sim 1.5$ at *STEREO B* compared with about 6 at *Wind*. Consequently, the shock strength is decreased with a density compression ratio of about 2 and magnetic field compression ratio of about 1.8 at *STEREO B* (compared with 3 for the density and 4 for the field at *Wind*). Efficiency in particle acceleration is expected to decrease, too. Second, the shock arrives at *STEREO B* around 04:55 UT on August 3, about 12 hr earlier than at *Wind*, although *STEREO B* is farther away from the Sun (1.06 AU). This indicates a non-spherical structure of the shock. A possible explanation is that CME1, whose propagation direction is east of the shock, may have removed some of the solar wind plasma ahead of the shock. The eastern flank of the shock is thus expected to move faster as it is propagating into a less dense medium. A closer look at Figures 4 and 5 also reveals a pronounced northward magnetic field component downstream the shock at *Wind* while a large southward field component behind the shock at *STEREO B*, presumably produced by the interaction between the shock and preceding ejecta.

In addition to the interaction of a shock with a preceding ejecta, we also observe two ICMEs (ICME2 and ICME3) behind the shock at *Wind* that seem to have already merged. Connections between the imaging observations and in situ measurements suggest that ICME2 and ICME3 correspond to CME2 and CME3, respectively, although other possibilities cannot be completely excluded. ICME2 is mainly identified from the rotation of the magnetic field and depressed proton β, while the identification of ICME3 is straightforward. A region with relatively enhanced proton density, temperature, and β is observed between ICME2 and ICME3. Presumably, this is the interface of the CME–CME interaction. The magnetic field polarity in this interaction region is opposite to those inside the two ejecta, so magnetic reconnection may have occurred. The interval of ICME2 is very short, and its temperature seems enhanced compared with a typical ICME at 1 AU. A possible explanation is that the shock driven by ICME3, which is probably shock2, has already passed through ICME2 at 1 AU. This explanation is consistent with imaging observations.

Compression by ICME3 from behind may also contribute to the heating and field enhancement in addition to shock compression. In situ measurements at *STEREO B* also indicate an ejecta-like structure behind the shock, whose identification is mainly based on the relatively enhanced magnetic field. Its plasma and magnetic field structure, however, is very complicated and does not qualify for a typical ICME. One ICME may miss *STEREO B*, or the merging of the two ICMEs is such that typical ICME signatures are no longer recognizable. The readers are directed to C. Möstl et al. (2012, in preparation) for more discussions on the in situ signatures.

3. SUMMARY

We have investigated CME–CME interactions, combining imaging observations with in situ measurements from multiple vantage points. With the advantage of having wide-angle imaging observations, we are able to follow how the patterns of interacting CMEs evolve with time and how the interaction features in images connect with in situ signatures. Two CMEs (CME2 and CME3) from 2010 August 1 merged around 55 solar radii from the Sun into a broad wave with enhanced brightness. Connections with in situ signatures suggest that the merged front is a shock, followed by two ejecta observed at *Wind* which seem to have already merged. The shock, which is probably driven by CME3, may have passed through CME2 well before 1 AU and is propagating into the CME from July 30 (CME1) near 1 AU. In situ measurements at 1 AU show that the preceding ejecta is significantly compressed, accelerated, and heated by the overtaking shock. The interaction also modifies the shock strength and structure on a global scale as indicated by additional measurements at *STEREO B*.

The research was supported by the *STEREO* project under grant NAS5-03131. C.M. is supported by a Marie Curie International Outgoing Fellowship. M.T. acknowledges the Austrian Science Fund FWF V195-N16.

REFERENCES

Burlaga, L. F., Plunkett, S. P., & St. Cyr, O. C. 2002, J. Geophys. Res., 107, 1266
Davies, J. A., Harrison, R. A., Rouillard, A. P., et al. 2009, Geophys. Res. Lett., 36, L02102
Dungey, J. W. 1961, Phys. Rev. Lett., 6, 47
Eyles, C. J., Harrison, R. A., Davis, C. J., et al. 2009, Sol. Phys., 254, 387
Farrugia, C., & Berdichevsky, D. 2004, Ann. Geophys., 22, 3679
Galvin, A. B., Kistler, L. M., Popecki, M. A., et al. 2008, Space Sci. Rev., 136, 437
Gopalswamy, N., Yashiro, S., Kaiser, M. L., Howard, R. A., & Bougeret, J.-L. 2001, ApJ, 548, L91
Gopalswamy, N., Yashiro, S., Michałek, G., et al. 2002, ApJ, 572, L103
Gosling, J. T., McComas, D. J., Philips, J. L., & Bame, S. J. 1991, J. Geophys. Res., 96, 7831
Harrison, R. A., Davies, J. A., Möstl, C., et al. 2012, ApJ, submitted
Harrison, R. A., Davis, C. J., Eyles, C. J., et al. 2008, Sol. Phys., 247, 171
Howard, R. A., Moses, J. D., Vourlidas, A., et al. 2008, Space Sci. Rev., 136, 67
Kaiser, M. L., Kucera, T. A., Davila, J. M., et al. 2008, Space Sci. Rev., 136, 5
Liu, Y., Davies, J. A., Luhmann, J. G., et al. 2010a, ApJ, 710, L82
Liu, Y., Luhmann, J. G., Bale, S. D., & Lin, R. P. 2011, ApJ, 734, 84
Liu, Y., Thernisien, A., Luhmann, J. G., et al. 2010b, ApJ, 722, 1762
Lugaz, N., Manchester, W. B., IV, & Gombosi, T. I. 2005, ApJ, 634, 651
Luhmann, J. G., Curtis, D. W., Schroeder, P., et al. 2008, Space Sci. Rev., 136, 117
Martinez-Oliveros, J. C., Raftery, C. L., Bain, H. M., et al. 2012, ApJ, submitted
Möstl, C., Temmer, M., Rollett, T., et al. 2010, Geophys. Res. Lett., 37, L24103
Richardson, I. G., Lawrence, G. R., Haggerty, D. K., Kucera, T. A., & Szabo, A. 2003, Geophys. Res. Lett., 30, 8014
Schmidt, J. M., & Cargill, P. J. 2004, Ann. Geophys., 22, 2245
Schrijver, C. J., & Title, A. M. 2011, J. Geophys. Res., 116, A04108
Sheeley, N. R., Herbst, A. D., Palatchi, C. A., et al. 2008, ApJ, 675, 853
Temmer, M., Vrsnak, B., Rollet, T., et al. 2012, ApJ, submitted
Vandas, M., Fischer, S., Dryer, M., et al. 1997, J. Geophys. Res., 102, 22295
Wang, Y. M., Ye, P. Z., & Wang, S. 2003, J. Geophys. Res., 108, 1370
Xiong, M., Zheng, H., Wang, Y., & Wang, S. 2006, J. Geophys. Res., 111, A08105